Kwon *et al.*
Journal of Analytical Science and Technology (2022) 13:14
https://doi.org/10.1186/s40543-022-00323-8

Journal of Analytical Science and Technology

TECHNICAL NOTE

Open Access

Abnormal shadow contrast imaging for optimal objective lens condition in transmission electron microscope

Yong-Eun Kwon, Cheolsu Han, Sang-Chul Lee, Jong-Man Jeung, Gaehang Lee, Tae-Yeoung Lee and Jin-Gyu Kim*

Abstract

Background: In a transmission electron microscope (TEM), the objective lens (OL) is the most important component because the first image and diffraction pattern for a specimen are formed by applying a specific OL current and specimen height (SH). In TEM, the focal length of the OL should be controlled independently of the specimen position. Therefore, the initial conditions for OL should be determined by selecting the optimum imaging condition of the specimen based on the OL current and the specimen position. We would like to present a method for finding the optimal imaging condition for OL that can be applied to conventional or low-resolution TEM where high-resolution (HR) imaging is impossible.

Findings: We conducted an abnormal contrast imaging experiment using Au nanoparticles (AuNPs). Abnormal contrast imaging was obtained by artificially controlling the mechanical alignment of OL P/Ps. Abnormal contrasts (shadow contrasts) of AuNPs were observed in all images obtained for various SH and OL currents. It was confirmed that these shadow contrasts of AuNPs result from the parasitic aberration caused by imperfect mechanical alignment of the OL P/Ps. From the quantitative analysis of the images, it was found that the effects of parasitic aberration in the TEM images decreased as SH approached the optimal position in the OL P/P.

Conclusion: We examined the relationship of SH and OL current using the abnormal contrast imaging technique. The standard OL current and optimal SH were determined with OL condition minimizing the shadow contrast of images. The experimentally determined optimal SH at standard OL current in our specially designed OL system differed from that of the well-known asymmetry OL system. Therefore, it is essential to examine the optimum conditions from a practical perspective. Consequently, our abnormal contrast imaging method, which can be analyzed even in conventional imaging without HR-TEM performance, can help optimize the OL conditions during the manufacturing stage of the TEM instrument.

Keywords: TEM, Abnormal contrast imaging, Standard objective lens, Specimen height, Shadow contrast

Introduction

Transmission electron microscope (TEM), an essential imaging tool for investigating the structural and chemical characteristics of nano-sized materials, comprises electromagnetic lenses such as condenser lens, objective lens (OL), intermediate lens, and projector lens. The OL is the most important lens in TEM because the first image and diffraction pattern for the specimen are formed by the interaction of electrons and the specimen under specific excitation conditions of an OL (Williams and Carter 2009).

Generally, three major parameters are considered when determining the optimum imaging condition

*Correspondence: jjintta@kbsi.re.kr
Center for Scientific Instrumentation, Korea Basic Science Institute, Daejeon 34133, Republic of Korea

with the OL. First, the standard OL current forming the maximum image contrast of the specimen. Second, the specimen height (SH) in the pole-piece (P/P) gap. Finally, an objective aperture position between the upper and lower P/Ps for the back-focal plane (BFP) forming the electron diffraction.

The objective aperture position in the P/P gap can be easily determined by calculating the BFP of the OL with the specific OL currents. Conversely, the OL current and SH are dependent on each other. Furthermore, unlike glass lenses, the OL has an adjustable focal length that can be adjusted on the specimen position and vice versa. Therefore, it is necessary to determine the initial conditions for the best instrument performance based on the OL current and specimen position.

In conventional TEM, the specimen is located at the center and one-third of the P/P gap in symmetric and asymmetric OL type, respectively (De Graef 2003; Hawkes et al. 1982). Moreover, the OL conditions for minimum optical aberrations (spherical and chromatic aberration) were reported by computational studies (Mulvey and Wallington 1969; Spence 2003).

However, the more accurate SH varies based on the actual geometry and lens excitation properties of the OL. Therefore, the optimum SH must be determined by trial and error. A simple procedure is to obtain images of specimen for a range of SH and to select the best quality image by eye and computer image-matching technique (Barry 1992; Spence 2003). However, it is difficult to apply these procedures when low contrast specimens are used or high-resolution imaging is not possible. To overcome this problem, in this study, we experimentally determined the optimal SH in the OL P/P gap using abnormal shadow imaging of spherical nanoparticles.

Experimental methods

We used a recently developed in-house low-voltage TEM (Max. 30 kV) comprising a thermal emission electron gun (W or LaB_6), and an electromagnetic optical lens system consisting of two condenser lenses, an OL, three intermediate lenses, and a projection lens.

Au nanoparticles (AuNPs) having a size of 40 nm were used as the sample for this study. The AuNPs were synthesized by a growth and selective etching process using gold (III) chloride trihydrate ($HAuCl_4$, 49.0% metal basis), ethylene glycol (EG, anhydrous, 99.8%), phosphoric acid (H_3PO_4, 85 wt% in H_2O), and poly (dimethyldiallylammonium chloride) (polyDADMAC, molecular weight: 400–500 K, 20 wt% in H_2O), purchased from Sigma-Aldrich (USA) (Lee et al. 2013).

To determine the optimal SH, we selected 10 specimen positions along the optic axis in the OL P/P gap. The TEM images of the AuNPs were obtained using a side-entry CMOS camera (PHURONA, EMSIS GmbH), by considering the appropriate OL current values corresponding to each SH.

Digital micrograph (Gatan Inc.) software was used for image processing and line profile analysis of shadow contrast of TEM images. The contrast transfer function (CTF) of the OL was calculated using exCTF simulator (Lee et al. 2020). The optical simulations for the specific OL were performed using Munro's Electron Beam Software (MEBS) (Munro et al. 2006). The magnetic fields, lens excitation, and focal lengths were calculated based on the actual specifications of the OL, such as coil windings, OL currents, and P/P materials.

Results and discussion

Figure 1 shows the basic optical properties of the OL used in this study. The geometry and isopotential lines of OL are shown in Fig. 1a. The P/P structure of the OL has an

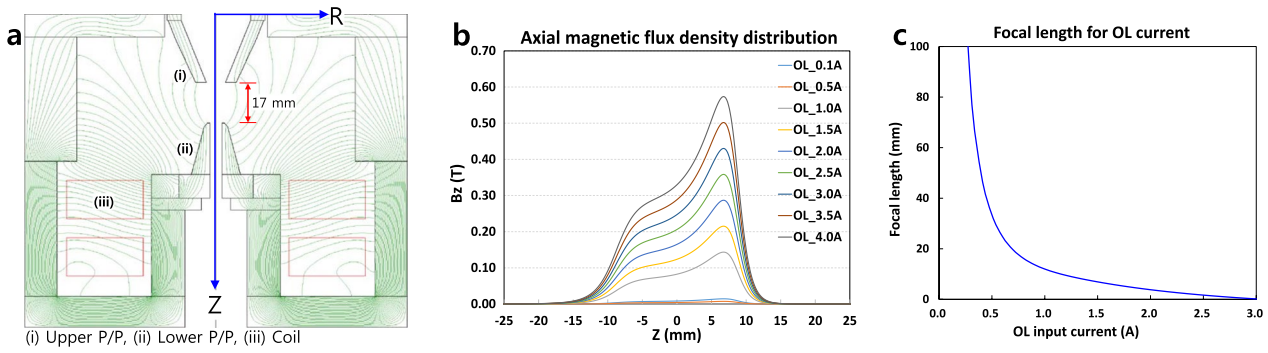

Fig. 1 The OL property of the developed low-voltage TEM. **a** P/P structure and its equi-flux density. **b** Axial magnetic flux density distribution for various input OL currents. **c** Focal length according to input OL currents

asymmetric type with a gap of 17 mm. Moreover, Z and R in Fig. 1a denote the optical axis direction and radius direction from the optic axis of the lens, respectively. The contour lines represent the equi-flux density in the magnetic circuit. The maximum value is 2.61×10^{-3} Tesla (T), and the interval of the contour lines is 6.66×10^{-5} T. Furthermore, the red boxes represent the magnetic coil windings area for calculating the current density.

Figure 1b shows the axial magnetic flux density (B_z) distribution for various input OL currents. With the center of the P/P gap as 0 mm on Z-direction, the upper P/P and lower P/P are located at z = -8.5 mm and z = 8.5 mm, respectively. Note that the maximum values of axial magnetic flux density increase as the input OL currents, except for lower input OL currents of 0.1 A and 0.5 A, increase. The positions of the maximum value of B_z for various OL currents were maintained constant in the Z-direction. However, the shape of the B_z distribution was not a Gaussian distribution but a two-shoulder distribution which may be due to its extremely wide P/P gap and P/P geometry. The focal lengths of the OL currents were calculated using a built-in MEBS procedure, as shown in Fig. 1c. The effective OL currents ranged from 0.77 A to 3.00 A based on their P/P geometry and OL excitation for beam focusing.

The acquisition conditions for the experimental images are listed in Table 1. First, we examined the adjustable Z-axis range of the TEM goniometer and determined the movable range to be 3 mm at 6 mm from the top of the lower P/P. Generally, the goniometer geometry for vacuum and motor control methods limits the adjustable Z-axis range to approximately 1 mm in almost all commercial TEM. However, in this study, the adjustable Z-axis range was sufficient for determining the optimal SH. The SH was controlled between 6 and 9 mm from the top of the lower P/P, and 10 SH positions were examined with 0.33 mm steps. In addition, we also presented the corresponding OL currents to determine the best contrast images.

Figure 2 shows a series of experimental images regarding the variation in SH in the P/P gap. All images obtained at various SH were focused by applying their

Table 1 SH setting conditions and their corresponding OL current values, magnitude of length, and rotation angle of the shadow contrast

Image Number	1	2	3	4	5	6	7	8	9	10
SH position from the top of the lower pole piece (mm)	6.00	6.33	6.67	7.00	7.33	7.67	8.00	8.33	8.66	9.00
OL current (A)	2.027	1.978	1.884	1.802	1.739	1.672	1.621	1.587	1.523	1.481
Length of the shadow contrast (nm)	84.2	68.6	64.1	38.5	29.7	26.6	25.0	24.2	30.8	33.1
Rotation angle (°)	1.3	14.0	21.1	29.6	41.0	45.8	52.6	57.8	67.5	71.6

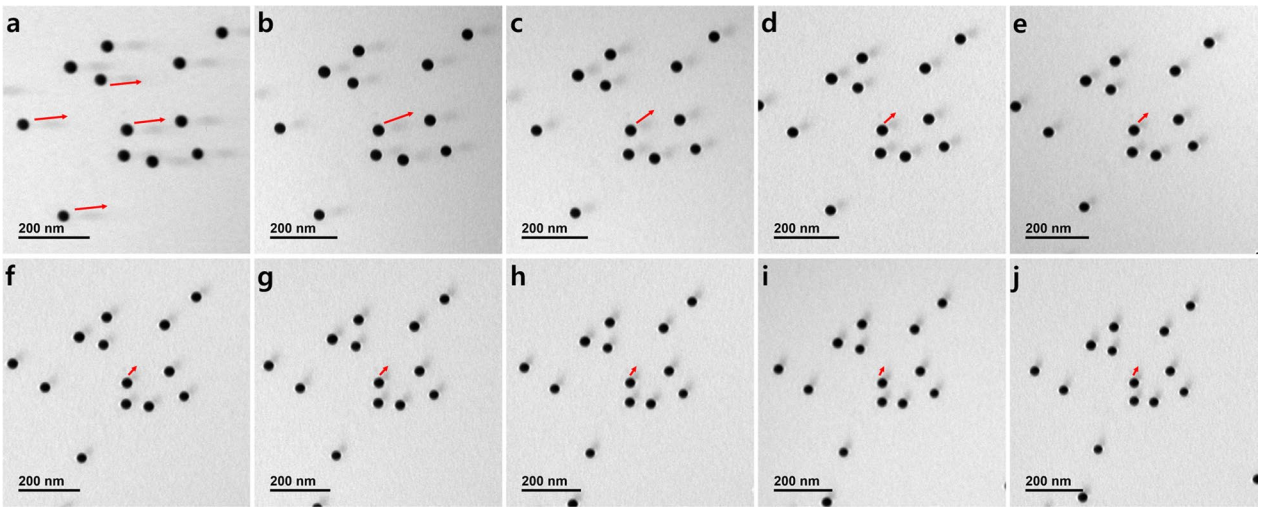

Fig. 2 Experimental images of 10 different SH positions. The SH was adjusted at intervals of 0.33 mm between 6 and 9 mm from the top of the lower P/P. Each image from (**a**) to (**j**) was focused with an appropriate OL current for 10 SH positions. The red arrows indicate the direction of the shadow contrasts formed from AuNPs

corresponding OL currents. However, all images show abnormal contrasts (shadow contrasts) unrelated to the unique characteristics of the AuNPs, indicated by red arrows in the figure. These shadow contrasts should be eliminated as they cause confusion in the TEM image analysis. The shadow contrasts were maintained in a specific direction in the same TEM image and rotated in a series of images for various SHs. These results were due to the change in magnetic flux density for each OL current. If these shadow contrasts of AuNPs are caused by specific aberrations of the OL lens, it will be crucial to find OL conditions minimizing this aberration. In addition, as shown in Fig. 2a–j, the size of the AuNPs decreases as the angular magnification increases, due to a decrease in the OL current.

For quantitative analysis, the measurement results of the shadow contrasts of AuNPs are shown in Fig. 3. In particular, Fig. 3a shows the AuNPs image obtained at an SH of 6 mm (h6.00) from the top of the lower P/P. The origin point was determined in the x-axis direction of the coordinate of an AuNP to measure the rotation angle of the shadow contrast. The length of shadow contrast was compared by measuring the length by tracking the same particle in each image. The actual distance was calculated by applying calibrated scale of the magnification to the measured number of pixels using Digital micrograph (Gatan Inc.) software.

The length and rotation angle of the shadow contrast are shown in Fig. 3b. The shadow contrasts rotated from the h6.00 to the h9.00 position with a variation in the OL currents. In contrast, the length of the shadow contrast gradually decreases and is the shortest at h8.33. Table 1 shows the final results of the shadow contrast of AuNPs. The longest shadow contrast (84.2 nm) at h6.00 decreased to 24.2 nm at h8.33. Consequently, the optimal specimen position can be regarded as the approximate central point of the P/P gap with a width of 17 mm.

As mentioned in the introduction, we assumed that the specimen was located at the center and one-third from the center of the upper and lower P/Ps in symmetric and asymmetric OL type, respectively (De Graef 2003; Hawkes et al. 1982). However, the optimal SH determined in our asymmetric OL exhibited the characteristics of symmetric OL. This is due to the two-shoulder distribution of B_z formed by the relatively wide P/Ps gap and the shape of the P/Ps as mentioned in Fig. 1. The behavior of the electron beam affected by this particular B_z distribution unexpectedly changes the optimal specimen position in the P/Ps gap. Therefore, to determine the optimal imaging conditions for the OL current and SH, it is essential to comprehensively consider the geometry, axial magnetic flux density, and focal length of an OL.

Additional experiments were performed to verify the usefulness of the proposed method. First, to understand the cause of shadow contrast, we adjusted the mechanical alignment between the upper and the lower P/Ps of the OL (Fig. 4). Figure 4a shows the direction of the mechanical misalignment between upper and lower P/Ps in the OL. The lower P/P was fixed at the central position, and the upper P/P was misaligned while moving a certain distance in the radial y-axis (R_y) direction. Figure 4b shows the shadow contrast of AuNPs according

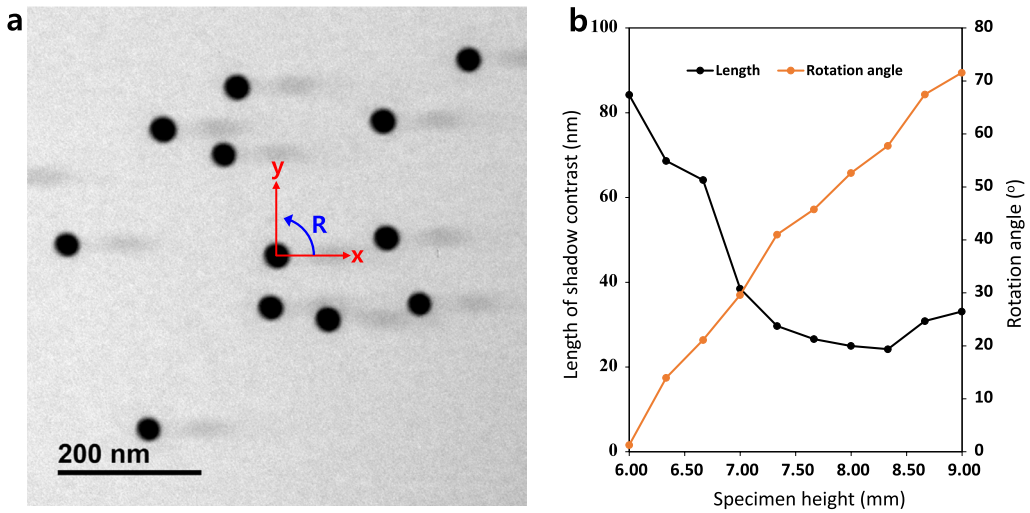

Fig. 3 Analysis of the shadow contrast images. **a** Specimen image obtained at an SH of 6 mm from the top of the lower P/P. The x-axis direction represents the rotation origin of shadow contrast, and R represents the rotation direction. **b** Measurement results of the shadow contrast for each TEM image

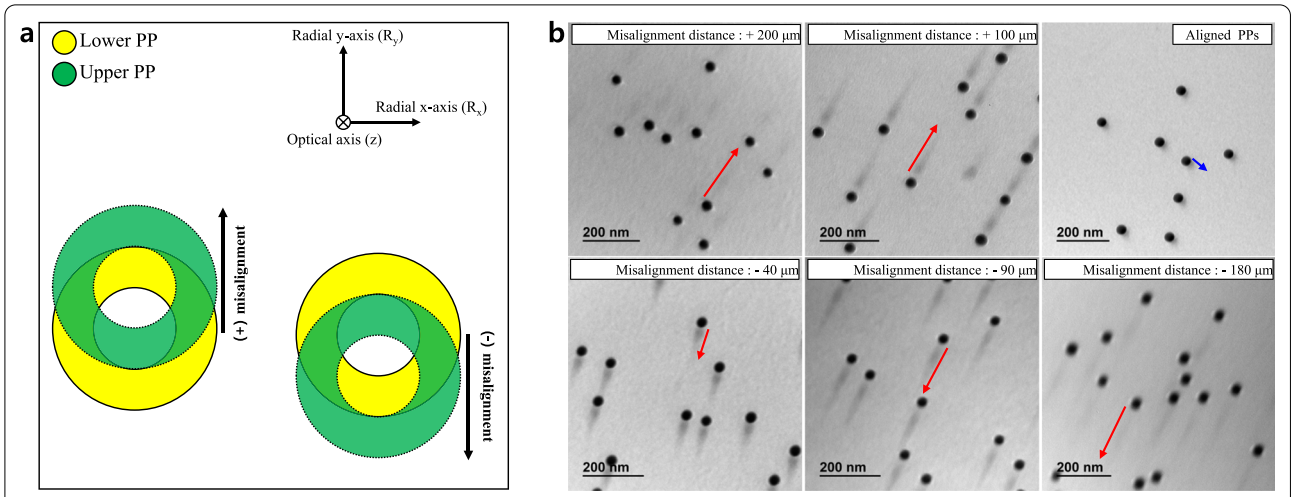

Fig. 4 Adjusting of mechanical alignment of OL P/Ps and thus shadow contrast imaging of AuNPs. **a** Schematic diagram of the mechanical alignment of OL P/Ps. **b** Shadow contrast imaging of AuNPs according to the magnitude of mechanical misalignment of OL P/Ps. The length and direction of shadow contrast (red arrows) are proportional and considered to the magnitude and direction of OL P/Ps misalignment, respectively

to misalignment of OL P/Ps. The length of shadow contrast is proportional to the magnitude of misalignment, and the direction of shadow contrast (red arrows) is also considered to be along the OL P/Ps misalignment direction. The shadow contrast (blue arrow) shown for the aligned P/Ps in Fig. 4b is due to misalignment of the OL P/Ps in the radial x-axis (R_x component) direction. The parasitic aberrations, not inherent aberrations like five Seidel aberrations, arise from mechanical problems such as magnetic non-uniformity of the P/P material, machining inaccuracy of the P/P, and disagreement of the optical axes between lenses in TEM (Jon 2009; Tanaka 2021). Consequently, the shadow contrast in our experiments results from the parasitic aberration (axial coma aberration) caused by misalignment of OL P/Ps. Furthermore, the magnitude of shadow contrast can be artificially adjusted through fine-tuning of the mechanical alignment of the OL P/Ps.

Subsequently, to confirm whether the optimal OL condition changes according to the magnitude of parasitic aberration, we performed imaging of AuNPs and analyzed by changing the condition of the misalignment of OL P/Ps (Fig. 5). The SH and OL currents for each of the obtained images were the same as for the images in Fig. 2. Figure 5a shows the images of AuNPs obtained by minimizing misalignment of OL P/Ps for 1-axis (R_y) with reference to Fig. 4a. That is, Fig. 5a shows images obtained for a series of SH for the aligned P/Ps in Fig. 4b. Additionally, Fig. 5b shows images of AuNPs obtained after performing the 2-axis alignment of OL P/Ps (both R_y and R_x), and the residual shadow contrast (blue arrow) in Fig. 5a was minimized. The results of measuring the length of shadow contrast for each AuNPs image are shown in Fig. 5c. Although the optimal SH position (h8.00) in the OL P/Ps differs by 0.33 mm from the result (h8.33) obtained in Fig. 3c, the relationship between the length of shadow contrast and SH shows a similar trend in three different mechanical alignment cases of OL P/Ps. Consequently, the initial condition of OL can be established by creating an appropriate parasitic aberration through the mechanical alignment of OL P/Ps and finding the conditions for the SH and OL current minimizing the effect of the generated parasitic aberration. Unfortunately, the residual shadow contrasts still existed at the optimal SH, as shown in Figs. 2h and 5b, and it is expected to be removed using a more precise mechanical alignment tool.

Geometrical and chromatic aberrations of the lens are primary factors affecting the image resolution of TEM. Therefore, optimal OL condition is essential to select the conditions minimizing lens aberration. Simple and low-order aberrations (=up to 2nd-order Seidel aberrations) are corrected through a deflection system. However, complex and higher-order aberrations (chromatic and higher-order Seidel aberrations) are challenging to correct without a dedicated aberration corrector.

To simply check the effect of chromatic aberration coefficient (C_c) and spherical aberration coefficient (C_s) according to the OL condition, optical simulation of OL was performed (Fig. 6a). The C_c decreased as the OL current increased, while C_s was minimized when the OL current was approximately 1.4 A. The C_s and C_c for the OL current of 1.481 A (for h9.00) were 5.087 mm and 5.661 mm, respectively, and the C_s and C_c for the

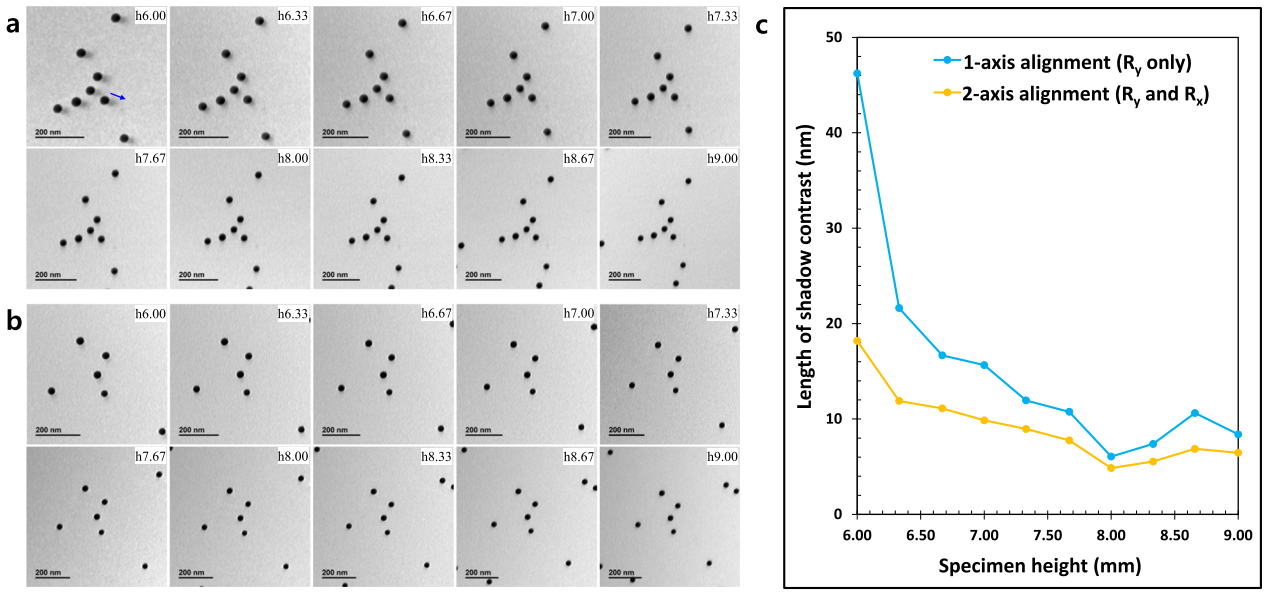

Fig. 5 Analysis results of imaging conditions of OL according to the mechanical alignment of OL P/Ps. **a** A series of shadow contrast images of AuNPs obtained for 1-axis alignment of OL P/Ps. **b** Shadow contrast images of AuNPs obtained after performing the 2-axes alignment of OL P/Ps. **c** Analysis results of the shadow contrast images for different SH positions

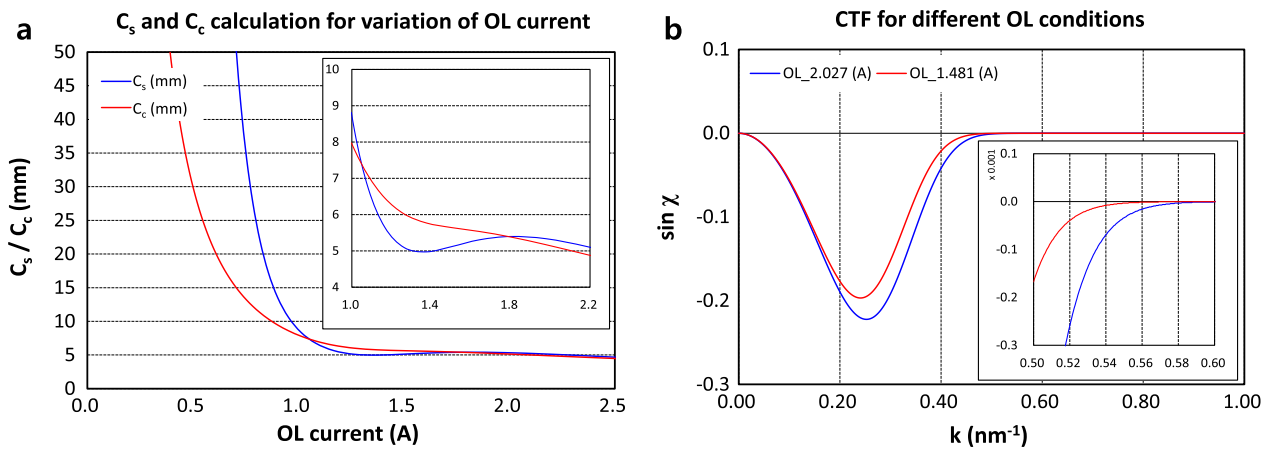

Fig. 6 **a** The calculation results of spherical and chromatic aberration coefficient for variation of OL current. **b** The CTF calculation results for two different OL conditions. Each inset in (**a**) and (**b**) represents a specific range of results for detailed information

OL current of 2.027 A (for h6.00) were 5.298 mm and 5.109 mm, respectively. Additionally, the CTF was calculated from the simulation results (Fig. 6b). For each OL current of 1.481 A and 2.027 A, the minimum values of sin χ were -0.197 and -0.222 at $k = 0.241$ nm^{-1} and $k = 0.252$ nm^{-1}, respectively. Moreover, the information limits for two different OL conditions are 1.758 nm and 1.668 nm. Therefore, it can be expected that small changes in C_s and C_c according to different OL conditions have a negligible effect on image contrast.

Therefore, as an alternative method for determining the optimal OL condition in conventional TEM or low-resolution TEM, which cannot experimentally measure chromatic and Seidel aberrations, we observed the artificial parasitic aberration using abnormal shadow contrast imaging and confirmed that the parasitic aberration could be minimized by adjusting the SH and OL currents. Therefore, setting the optimal SH and standard OL current using abnormal shadow contrast imaging can be helpful to determine the initial condition of prototype equipment and optimize the OL alignment.

Conclusions

In this study, we examined the optimum condition of SH and OL current using the abnormal contrast imaging technique. The optimal OL condition was determined with minimization of the shadow contrast formed by parasitic aberration as a condition. Although the origins of parasitic and Seidel aberrations are different, low-order Seidel and parasitic aberrations have more influence on image contrast in low-magnification or low-resolution imaging; therefore, they are an alternative to finding the optimum OL condition. In addition, the experimentally determined optimal SH at standard OL current in our OL system differed from that of the well-known asymmetry OL system. Therefore, it is essential to examine the optimum conditions from a practical perspective as well as optical simulation. Consequently, our abnormal contrast imaging method, which can be applied in low-resolution or conventional TEM, can help optimize the OL conditions during the manufacturing stage of the TEM instrument.

Abbreviations

TEM: Transmission electron microscope; OL: Objective lens; SH: Specimen height; P/P: Pole piece; HR-TEM: High-resolution TEM; BFP: Back-focal plane; AuNPs: Au nanoparticles; MEBS: Munro's Electron Beam Software; B_z: Magnetic flux density; C_s: Spherical aberration coefficient; C_c: Chromatic aberration coefficient; CTF: Contrast transfer function.

Acknowledgements

This study was supported by the Korea Basic Science Institute (Institutional Program: D210400).

Author contributions

JGK designed the research and wrote the manuscripts. YEK carried out the TEM experiment and analysis. CH, SCL, JMJ, and TYL developed the TEM optical devices and GUI. GL synthesized the test sample and characterized. All authors have read and approved the final manuscript.

Funding

This study was funded by the Korea Basic Science Institute (Institutional Program: D210400).

Availability of data and materials

Data sharing is not applicable to this article as no datasets were generated or analyzed during the current study.

Declarations

Competing interests

The authors declare that they have no competing interests.

Received: 15 December 2021 Accepted: 19 April 2022
Published online: 02 May 2022

References

Barry JC. Image-Matching as a means of atomic structure evaluation in high-resolution transmission electron microscopy. Scan. Microsc. 1992;1992(6): article 20. https://digitalcommons.usu.edu/microscopy/vol1992/iss6/20

De Graef M. Introduction to conventional transmission electron microscopy. 2nd ed. Cambridge: Cambridge University Press; 2003. p. 199–201.

Hawkes PW, Kasper E, Lenz F, Riecke WD, Mulvey T. Topics in current physics. In: Magnetic electron lenses. Berlin: Springer; 1982, p. 119–28.

Jon O. Aberrations. In: Handbook of charged particle optics. 2nd ed. Boca Raton: CRC Press; 2009, p. 210–339

Lee YJ, Schade NB, Sun L, Fan JA, Bae DR, Mariscal MM, Lee GH, Capasso F, Sacanna S, Manoharan VN, Yi GR. Ultrasmooth, highly spherical monocrystalline gold particles for precision plasmonics. ACS Nano. 2013;7:11064–70. https://doi.org/10.1021/nn404765w.

Lee SC, Jeung JM, Lee SG, Kim JG. exCTF simulator: Simulation tool for phase contrast transfer function for aberration-corrected transmission electron microscopy. J Anal Sci Technol. 2020;11:1–9. https://doi.org/10.1186/s40543-020-00231-9.

Mulvey T, Wallington MJ. The focal properties and aberrations of magnetic electron lenses. J Phys E: Sci Instrum. 1969;2:466–72. https://doi.org/10.1088/0022-3735/2/6/302.

Munro E, Rouse J, Liu H, Wang L, Zhu X. Simulation software for designing electron and ion beam equipment. Microelectron Eng. 2006;83(4–9):994–1002. https://doi.org/10.1016/j.mee.2006.01.076.

Spence JCH. High-resolution electron microscopy. 3rd ed. New York: Oxford University Press; 2003. p. 401.

Tanaka M. Glossary of TEM terms. Website of JEOL Ltd.; 2021. https://www.jeol.co.jp/en/words/emterms/search_result.html?keyword=parasitic+aberration

Williams DB, Carter CB. The instrument. In: Transmission electron microscopy, 2nd edn. Springer, New York; 2009, p. 141–69.

Publisher's Note